Electronic Supplementary Information

Utilization of Electron-Donating Linkers in M-Series Dimerized Acceptors to Achieve High-Voltage and Efficient Organic Solar Cells

Sihan Chen, Huixiang Jiao, Shuo Wan, Yi Li, Fangcong Zhang, Tianyu Hu, Wenwu Zhou, Huiting Fu, Qingdong Zheng*

State Key Laboratory of Coordination Chemistry, College of Engineering and Applied Sciences, Nanjing University, Nanjing 210023, China

Materials

PM6 and poly[(9,9-bis(3'-(N,N-dimethylamino)propyl)-2,7-fluorene)-alt-5,5'-bis(2,2'-thiophene)-2,6-naphthalene-1,4,5,8-tetracaboxylic-N,N'-di(2-ethylhexyl)imide](PNDIT-F3N) were purchased from Solarmer Materials Inc. (2-(9H-carbazol-9-yl)ethyl)phosphonic acid (2PACz) was purchased from Tokyo Chemistry Industry (TCI) Co. 2-(5-Bromo-3-oxo-2,3-dihydro-1H-inden-1-ylidene)malononitrile (IC-Br) and 2-(5,6-difluoro-3-oxo-2,3-dihydro-1H-inden-1-ylidene)malononitrile (IC-2F) were purchased from Suna Tech Inc. 2,5-Bis(trimethylstannyl)-3,4-ethylenedioxythiophene, 2,5-bis(trimethylstannyl)thiophene, and 2,5-bis(trimethylstannyl)-3,4-dimethoxythiophene were purchased from Nanjing Zhiyan Technology Co., Ltd. The three DSMAs were synthesized according to the procedures described below. Unless otherwise noted, all starting materials and solvents were purchased from commercial suppliers and used without further purification.

Synthesis

BPT-CHO (Compound **1**) was synthesized according to the previously reported literature.[S1-S2]

Synthesis of Compound 2: BPT-CHO (400 mg, 0.32 mmol) and 2-(5-bromo-3-oxo-2,3-dihydro-1H-inden-1-ylidene)malononitrile (IC-Br) (113 mg, 0.42 mmol) were dissolved in 20 mL of toluene, and 0.4 mL of acetic anhydride and 0.2 mL of boron trifluoride diethyl etherate were added sequentially after the reactants were fully dissolved. The reaction was allowed to proceed for one hour at room temperature. Then, the reaction mixture was poured into methanol and the precipitate was filtered off. The crude product was purified by silica gel column chromatography (200-300 mesh) using petroleum

ether/dichloromethane (1:1, v/v) as the eluent. The product was obtained as a black solid in 65% yield. **Compound 2**: ^{1}H NMR (400 MHz, Chloroform-d): δ 9.96 (s, 1H), 8.98 (s, 1H), 8.54 (d, *J* = 8.4 Hz, 1H), 8.02 (d, *J* = 2.0 Hz, 1H), 7.94 (s, 1H), 7.84 (dd, *J* = 8.4, 2.0 Hz, 1H), 7.73 (s, 1H), 4.75 (d, *J* = 7.6 Hz, 4H), 4.01 (t, *J* = 7.2 Hz, 4H), 2.13 – 1.97 (m, 4H), 1.65 (s, 4H), 1.42 – 0.74 (m, 100H).

Synthesis of Compound 3a: In a 100 mL two-necked round-bottomed flask, compound 2 (313 mg, 0.21 mmol), 2,5-bis(trimethylstannyl)-3,4-ethylenedioxythiophene (39 mg, 0.08 mmol), $Pd_2(dba)_3$ (19 mg, 0.02 mmol), and $P(o\text{-}tol)_3$ (24 mg, 0.08 mmol) were added. The reaction system was evacuated-nitrogen-filled three times. Then 50 mL of toluene that had been deoxygenated for 20 min was added. The mixture was stirred at 110 ℃ for 5 h. Upon completion of the reaction, 20 mL of methanol was added, and the solvent was removed under reduced pressure using a rotary evaporator. The residue was purified by silica gel column chromatography (PE/DCM, 1/1.5, v/v). Recrystallization from a mixture of chloroform and methanol afforded the final product as a black solid in 75% yield after suction filtration. **Compound 3a**: ^{1}H NMR (400 MHz, Chloroform-d): δ 9.96 (s, 2H), 8.98 (s, 2H), 8.70 (d, *J* = 8.4 Hz, 2H), 8.40 (d, *J* = 1.2 Hz, 2H), 8.08 (dd, *J* = 8.0, 1.6 Hz, 2H), 7.91 (s, 2H), 7.73 (s, 2H), 4.76 (d, *J* = 7.6 Hz, 8H), 4.54 (s, 4H), 4.02 (t, *J* = 5.2 Hz, 8H), 2.14 – 1.97 (m, 8H), 1.67 (s, 8H), 1.43 – 0.69 (m, 200H).

Synthesis of Compounds 3b-c: Compounds 3b and 3c were synthesized and worked up using the same procedure as for compound 3a, but with 2,5-bis(trimethylstannyl)-3,4-dimethoxythiophene or 2,5-bis(trimethylstannyl)thiophene, respectively. The final products were obtained as black solids with yields of 66% and 71%, respectively. **Compound 3b**: ^{1}H NMR (400 MHz, Chloroform-d): δ 9.96 (s, 2H), 8.99 (s, 2H), 8.73 (d, *J* = 8.4 Hz, 2H), 8.36 (d, *J* = 2.4 Hz, 2H), 8.13 (dd, *J* = 8.4, 2.0 Hz, 2H), 7.92 (s, 2H), 7.73 (s, 2H), 4.76 (d, *J* = 7.6 Hz, 8H), 4.05-4.01 (m, 14H), 2.14 – 1.98 (m, 8H), 1.67 (s, 8H), 1.42 – 0.74 (m, 200H). **Compound 3c**: ^{1}H NMR (400 MHz, Chloroform-d): δ 9.96 (s, 2H), 8.98 (s, 2H), 8.73 (d, *J* = 8.4 Hz, 2H), 8.14 (d, *J* = 2.0 Hz, 2H), 8.02 – 7.89 (m, 4H), 7.73 (s, 2H), 7.64 (s, 2H), 4.76 (d, *J* = 7.6 Hz, 8H), 4.03 (dd, *J* = 7.2, 3.6 Hz, 8H), 2.17-1.97 (m, 8H), 1.67 (s, 8H), 1.44 – 0.74 (m, 200H).

Synthesis of DM-EDOT: A mixture of Compound **3a** (236 mg, 0.08 mmol) and 2-(5,6-difluoro-3-oxo-2,3-dihydro-1H-inden-1-ylidene)malononitrile (IC-2F) (64 mg, 0.28 mmol) was dissolved in 30 mL of toluene and stirred vigorously until complete dissolution was achieved. To this solution, acetic anhydride (0.2 mL) and boron trifluoride diethyl etherate (0.1 mL) were added sequentially. The

reaction was allowed to proceed at room temperature for 1 hour. Upon completion, the reaction mixture was poured into methanol, and the precipitate was collected by filtration. The crude product was purified by column chromatography on silica gel using a mixture of petroleum ether and dichloromethane (1:2, v/v) as the eluent. Further recrystallization from chloroform and methanol afforded the final product DM-EDOT as a black solid in a yield of 85%. ^{1}H NMR (400 MHz, Chloroform-d): δ 8.97 (d, *J* = 6.6 Hz, 4H), 8.71 (d, *J* = 8.4 Hz, 2H), 8.54 (dd, *J* = 9.9, 6.4 Hz, 2H), 8.39 (s, 2H), 8.08 (d, *J* = 8.8 Hz, 2H), 7.91 (s, 4H), 7.69 (t, *J* = 7.6 Hz, 2H), 4.75 (d, *J* = 7.6 Hz, 8H), 4.55 (s, 4H), 4.04 (d, *J* = 6.8 Hz, 8H), 2.15 – 2.00 (m, 8H), 1.67 (s, 8H), 1.39 – 0.74 (m, 200H). MS (MALDI-TOF) m/z: calcd. for $C_{206}H_{254}F_4N_{12}O_{10}S_9$, 3423.7293; found, 3423.7392.

Synthesis of DM-DMOT and DM-TH: DM-DMOT and DM-TH were synthesized and worked up using the same procedure as for DM-EDOT. The final products were obtained as black solids with yields of 80% and 82%, respectively. **DM-DMOT**: ^{1}H NMR (400 MHz, Chloroform-d): δ 8.98 (d, *J* = 13.4 Hz, 4H), 8.74 (d, *J* = 8.4 Hz, 2H), 8.54 (dd, *J* = 9.9, 6.4 Hz, 2H), 8.36 (s, 2H), 8.13 (d, *J* = 8.4 Hz, 2H), 7.92 (s, 4H), 7.69 (t, *J* = 7.6 Hz, 2H), 4.75 (d, *J* = 7.6 Hz, 8H), 4.05–4.01 (m, 14H), 2.15 – 1.99 (m, 8H), 1.67 (s, 8H), 1.42–0.74 (m, 200H). MS (MALDI-TOF) m/z: calcd. for $C_{206}H_{256}F_4N_{12}O_{10}S_9$, 3425.7251; found, 3425.7422. **DM-TH**: ^{1}H NMR (400 MHz, Chloroform-d): δ 8.98 (d, *J* = 11.6 Hz, 4H), 8.75 (d, *J* = 8.4 Hz, 2H), 8.54 (dd, *J* = 9.8, 6.4 Hz, 2H), 8.14 (s, 2H), 8.03 – 7.89 (m, 6H), 7.70 (t, *J* = 7.6 Hz, 2H), 7.64 (s, 2H), 4.76 (d, *J* = 7.6 Hz, 8H), 4.04 (d, *J* = 6.8 Hz, 8H), 2.15 – 2.00 (m, 8H), 1.68 (s, 8H), 1.44 – 0.74 (m, 200H). MS (MALDI-TOF) m/z: calcd. for $C_{204}H_{252}F_4N_{12}O_8S_9$, 3364.7204; found, 3364.7585.

Instruments and characterization

^{1}H NMR spectra were recorded using a Bruker AV-400 spectrometer in a deuterated chloroform solution at 298 K, unless specified otherwise. Chemical shifts are reported as δ values (ppm) with tetramethylsilane (TMS) as the internal reference. Matrix-assisted laser desorption/ionization time-of-flight mass spectrometry (MALDI-TOF-MS) was performed on a Bruker Daltonics UltrafleXtreme spectrometer to determine the molecular weight. Surface topography was investigated by atomic force microscopy (AFM) using a Bruker Dimension Icon SPM system. UV-vis absorption spectra were obtained from a Shimadzu spectrophotometer. Cyclic voltammetry (CV) was carried out on a CHI-604E electrochemical workstation in a three-electrode configuration at a scan rate of 100 mV s^{-1}. The

electrolyte was a nitrogen-saturated acetonitrile solution containing 0.1 M tetrabutylammonium hexafluorophosphate (Bu_4NPF_6). The working, counter, and reference electrodes were a platinum plate, a platinum wire, and an $Ag/AgNO_3$ electrode (0.1 M in acetonitrile), respectively. The reference electrode was calibrated against the ferrocene/ferrocenium redox couple, with the Fc/Fc^+ oxidation potential taken as -4.84 eV relative to the vacuum level. The HOMO and LUMO energy levels of the materials were calculated using the following equations:

$$E_{HOMO} = -(\varphi_{ox} + 4.84)\ eV$$

$$E_{LUMO} = -(\varphi_{red} + 4.84)\ eV$$

Where φ_{ox} is the onset oxidation potential vs. $Ag/AgNO_3$ and φ_{red} is the onset reduction potential vs. $Ag/AgNO_3$. The density functional theory (DFT) was applied using the Gauss software package on B3LYP/6-31G(d) level.

Device fabrication and characterization

The photovoltaic performances of three dimerized acceptors were investigated by using a conventional device structure of ITO/2PACz/PM6:DSMAs/PNDIT-F3N/Ag. ITO glass was ultrasonically cleaned with detergent, deionized water, ethanol, and isopropanol for 15 min each, then dried overnight in an oven. Then, all substrates were exposed to the ultraviolet/ozone treatment for 15 min before use. SAM solution was prepared by dissolving (2-(9H-carbazol-9-yl)ethyl)phosphonic acid (2PACz) in isopropanol (0.3 mg mL^{-1}). 40 μL of the SAM solution was dropped onto the ITO substrates and spin-coated at 3000 rpm for 30 s. The substrates were then annealed at 100 ℃ for 10 min. The active layer was fabricated using the layer-by-layer (LBL) deposition method. A solution of the donor polymer PM6 in chlorobenzene (CB) at a concentration of 9 mg mL^{-1}, and a solution of the acceptor in chloroform (CF) at 6 mg mL^{-1} with the addition of 0.5% (vol.%) 1-chloronaphthalene (1-CN) as an additive were prepared. To fabricate conventional bulk-heterojunction (BHJ) devices, the donor and acceptor materials (with a D/A weight ratio of 1:1) were dissolved in chloroform at a total concentration of 16 mg/mL, with 0.5 vol% 1-chloronaphthalene (1-CN) added as an additive. For the best-performance device, the donor solution was first spin-coated at 1500 rpm, and then the acceptor solution was spin-coated at 3000 rpm, after 20 min thermal annealing at 100 ℃. Later, PNDIT-F3N electron-transporting layer was spin-coated onto the active layer at 2700 rpm for 30 s. Finally, 100 nm of Ag was deposited onto the PNDIT-F3N electron-transporting layer by thermal evaporation at

pressure of 1.0×10^{-5} Pa. The active area of the devices is 0.042 cm^2.

Current density-voltage (*J-V*) characteristics were recorded in the glove box with a Keithley 2400 Source Measure Unit under room temperature. The photocurrent was tested under AM 1.5G illumination at 100 mW cm^{-2} using a solar simulator (Enlitech, SS-F5, Taiwan). The light intensity was calibrated using a standard Si solar cell. The external quantum efficiency (EQE) spectra were obtained on a commercial EQE measurement system (Enlitech, QE-R). The light intensity at each wavelength was calibrated by a standard single-crystal Si photovoltaic cell. Thermal stability was evaluated using devices with the structure ITO/ZnO/BHJ active layers/MoO_3/Ag, which were continuously heated at 65 °C in a nitrogen atmosphere. Light-soaking stability was tested on devices with the structure ITO/2PACz/LBL active layers/PNDIT-F3N/Ag by tracking the maximum power point (MPP) under continuous LED illumination (100 mW cm^{-2}) at 25 °C.

Calculation of the energy loss (E_{loss})

The E_{loss} of OSCs is defined as the difference between the bandgap (E_g) of the photoactive materials and the V_{oc} of the device, which can be classified into three parts:

$$E_{loss} = (E_g - qV_{oc}^{SQ}) + (qV_{oc}^{SQ} - qV_{oc}^{rad}) + (qV_{oc}^{rad} - qV_{oc}) = \Delta E_1 + \Delta E_2 + \Delta E_3$$

where the E_g is determined by the crossing point of the normalized absorption in films. ΔE_1 represents the unavoidable radiative recombination loss above the Shockley–Queisser limit and was calculated as $\Delta E_1 = E_g - qV_{oc}^{SQ}$, where V_{oc}^{SQ} is the open-circuit voltage in the Shockley–Queisser limit obtained from the optical bandgap. ΔE_2 corresponds to the additional radiative loss caused by sub-bandgap absorption and was determined from $\Delta E_2 = qV_{oc}^{SQ} - qV_{oc}^{rad}$, where V_{oc}^{rad} is the radiative-limit open-circuit voltage derived from the measured EQE spectrum of the device. Alternatively, ΔE_3 can be estimated from the electroluminescence external quantum efficiency (EQE_{EL}) according to $\Delta E_3 = -\frac{kT}{q} ln(EQE_{EL})$, where k is the Boltzmann constant and T is the absolute temperature. For the EQE_{EL} measurements, a digital source meter (Keithley 2400) was employed to inject electric current into the solar cells, and the emitted photons were collected by a Si diode (Hamamatsu s1337-1010BQ) and measured with a picoammeter (Keithley 6482).

Transient photocurrent (TPC) and transient photovoltage (TPV) measurements

In the TPC and TPV measurements, the OSCs were fabricated with the same method as mentioned above. The data were obtained by the all-in-one characterization platform, Paios (Fluxim AG, Switzerland).

Calculation of exciton dissociation efficiency

The exciton dissociation process in the photovoltaic devices was investigated by plotting the photocurrent density (J_{ph}) against the effective voltage (V_{eff}). Here, J_{ph} and V_{eff} are defined as $J_{ph} = J_L - J_D$ and $V_{eff} = V_0 - V_{appl}$, where J_D and J_L are the current densities under dark and illuminated conditions, respectively, V_{appl} is the applied bias voltage, and V_0 is the voltage at which $J_{ph} = 0$. The exciton dissociation efficiency was calculated as the ratio of the photocurrent density (J_{ph}) under short-circuit conditions to the saturation photocurrent density (J_{sat}). The J_{sat} value was determined by averaging the J_{ph} in the high V_{eff} region ($\geq$ 1.0 V in these cases).

Electron mobility and hole mobility measurements

The electron and hole mobilities of the PM6:DM-EDOT, PM6:DM-DMOT, and PM6:DM-TH blend films were determined using the space charge limited current (SCLC) method. Hole-only devices were fabricated with ITO/2PACz/active layer/MoO_3/Ag, while electron-only devices were constructed with ITO/ZnO/active layer/PNDIT-F3N/Ag architecture. The active layers were prepared using the same method as that used for the best-performance OSC fabrication. Device areas were fixed at 0.042 cm^2. A Keithley 2440 source measurement unit measured the current density (J). The SCLC hole/electron mobilities were calculated according to the following equation: $J = 9\varepsilon_0\varepsilon_r\mu V^2/8d^3$. Where ε_0 is the free-space permittivity (8.85×10^{-12} F m^{-1}), and ε_r is the relative dielectric constant of the active layer material, usually 2–4 for organic semiconductors, herein we used a relative dielectric constant of 3, μ is the carrier mobility, V is the voltage drop across the SCLC device ($V = V_{app} - V_{bi}$, where V_{app} is the applied voltage to the device and V_{bi} is the built-in voltage due to the difference in the work function of two electrodes. In the hole-only and electron-only devices, the V_{bi} values are 0.5 and 0.7 V, respectively). d is the thickness of the active layer. The film thickness was detected by a Bruker Dektak XT surface profilometer. The hole or electron mobility can be calculated from the slope of the $J^{1/2}$-V curves.

GIWAXS characterization

All samples for GIWAXS characterization were fabricated on ITO substrates coated with 2PACz. The two-dimensional patterns were acquired using a XEUSS 3.0 system at the Fujian Science & Technology Innovation Laboratory for Optoelectronic Information of China. Measurements were performed with an X-ray wavelength of 1.54 Å and an incident angle of 0.2°. The scattered X-rays were detected by a Dectris Eiger2 R 1M photon-counting detector. The coherence length was estimated by the Scherrer equation: $CCL = 2\pi K/\mathrm{FWHM}$, where FWHM is the full width at half-maximum of the peak, and K is a shape factor (0.9 was used here).

Additional Tables and Figures

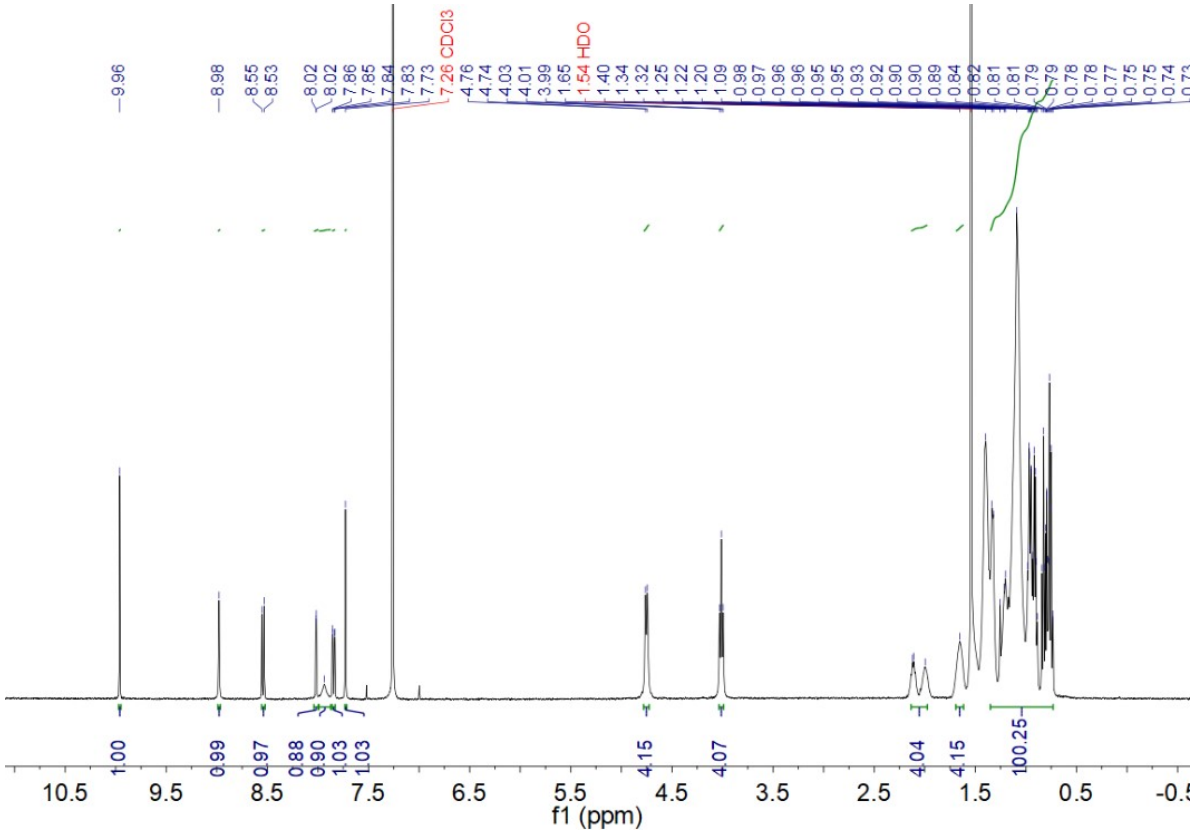

Figure S1. ^{1}H NMR spectrum of Compound **2** in $CDCl_3$.

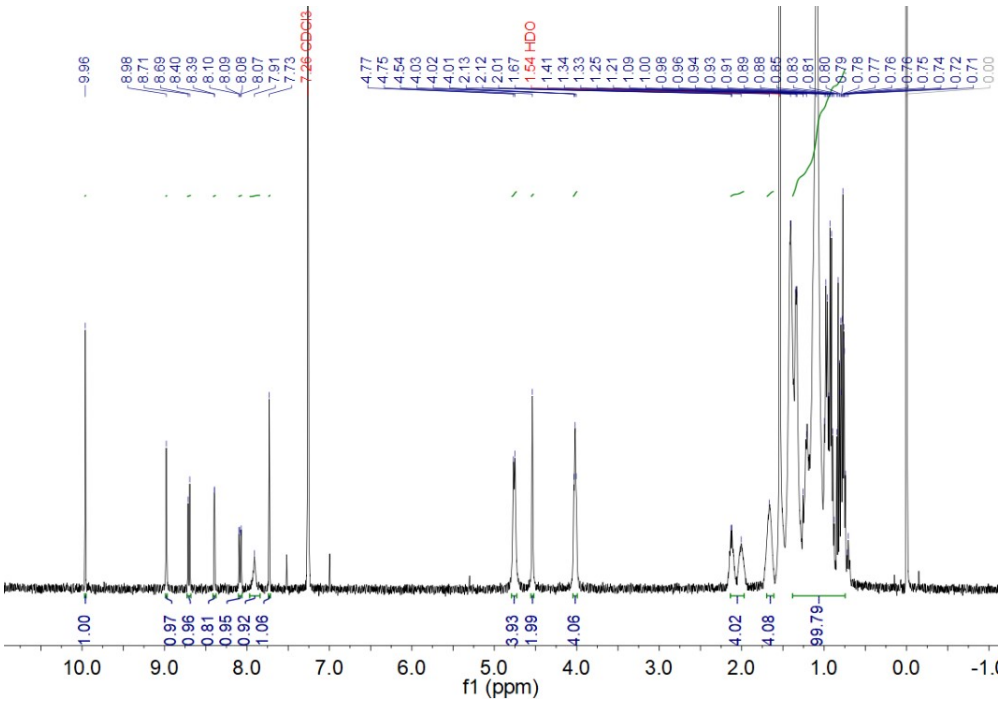

Figure S2. ^{1}H NMR spectrum of Compound **3a** in $CDCl_3$.

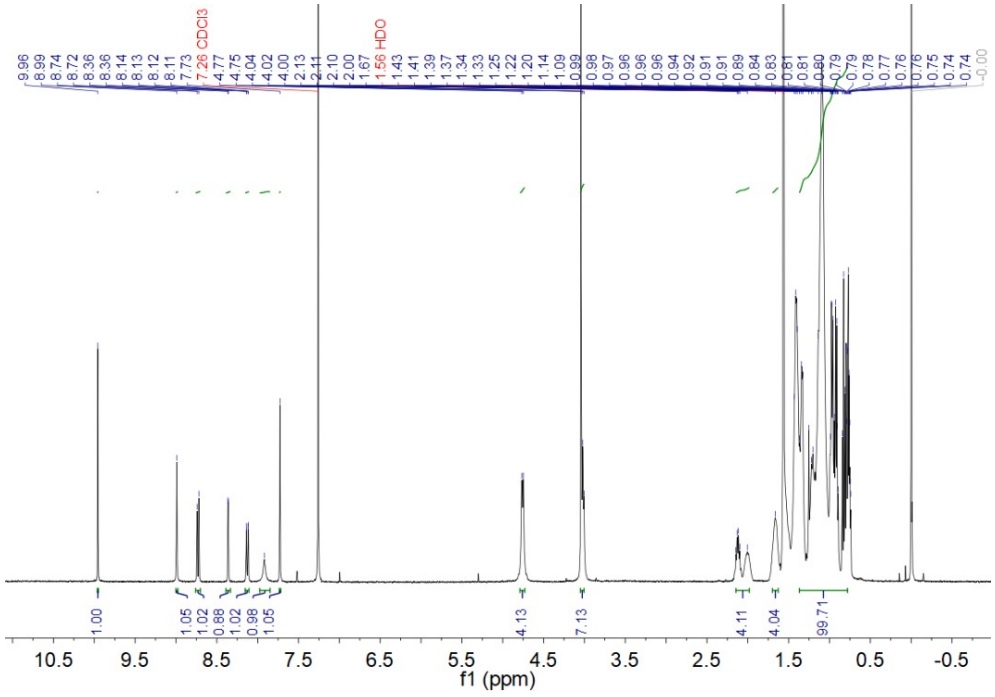

Figure S3. ^{1}H NMR spectrum of Compound **3b** in $CDCl_3$.

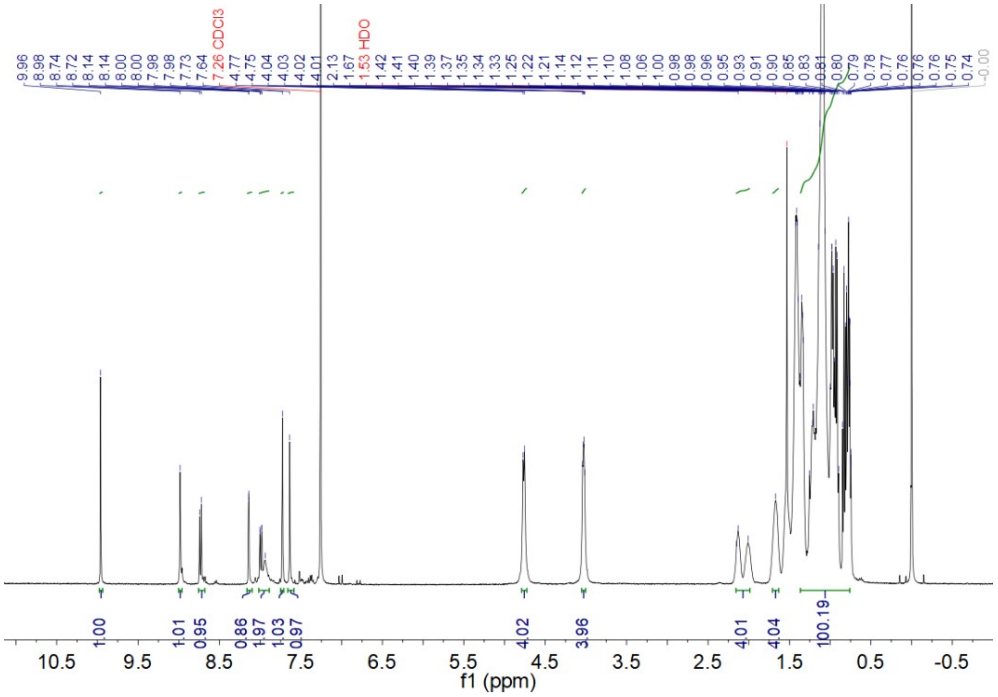

Figure S4. [1]H NMR spectrum of Compound **3c** in $CDCl_3$.

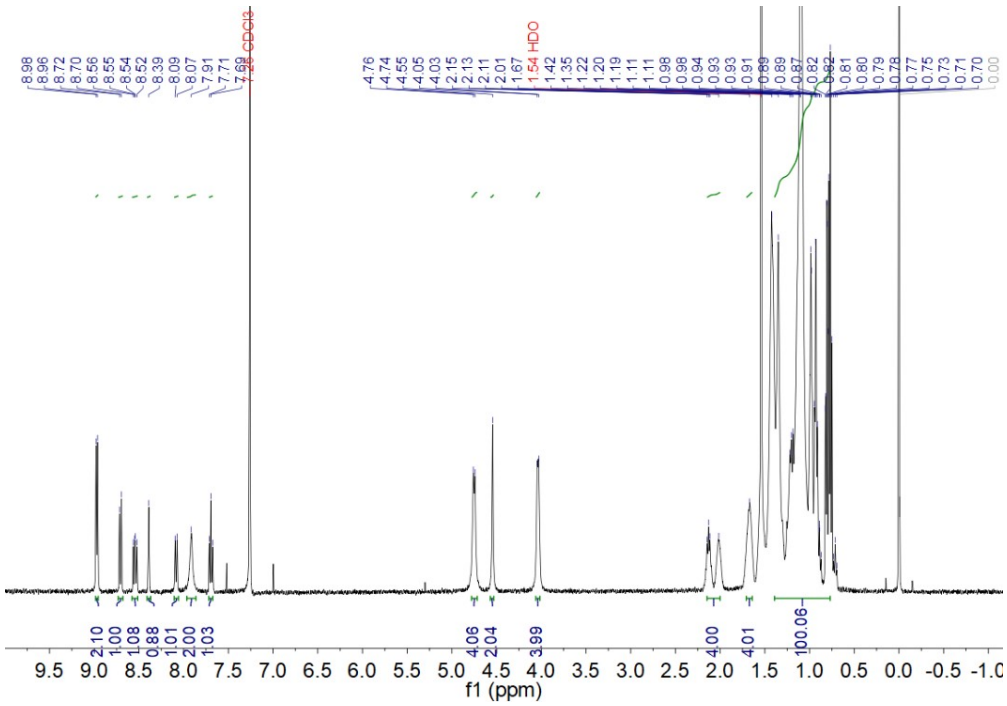

Figure S5. [1]H NMR spectrum of **DM-EDOT** in $CDCl_3$.

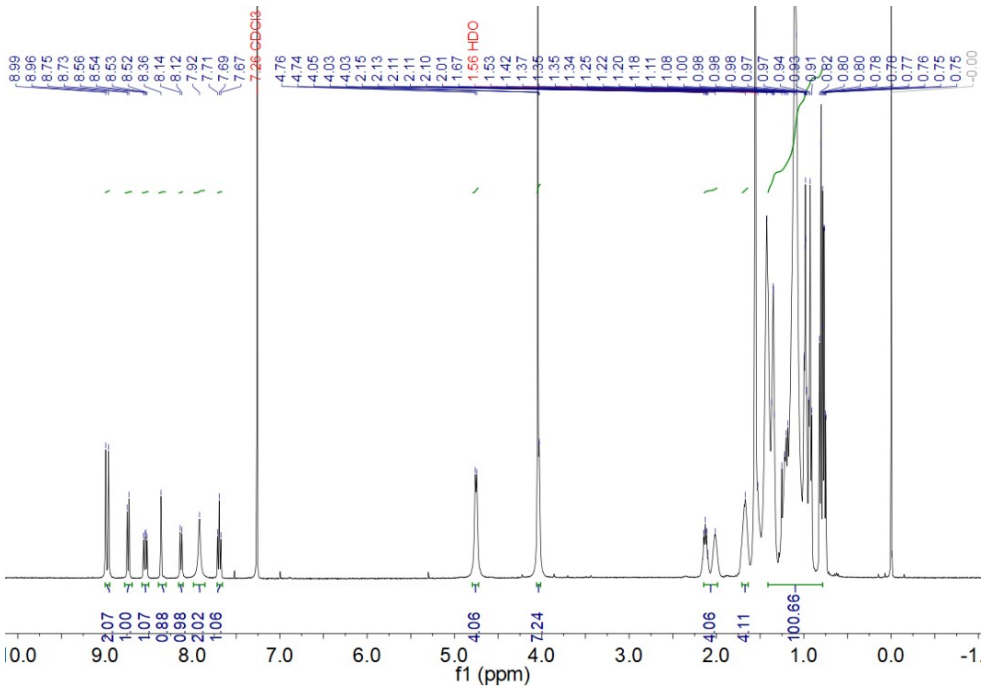

Figure S6. ^{1}H NMR spectrum of **DM-DMOT** in $CDCl_3$.

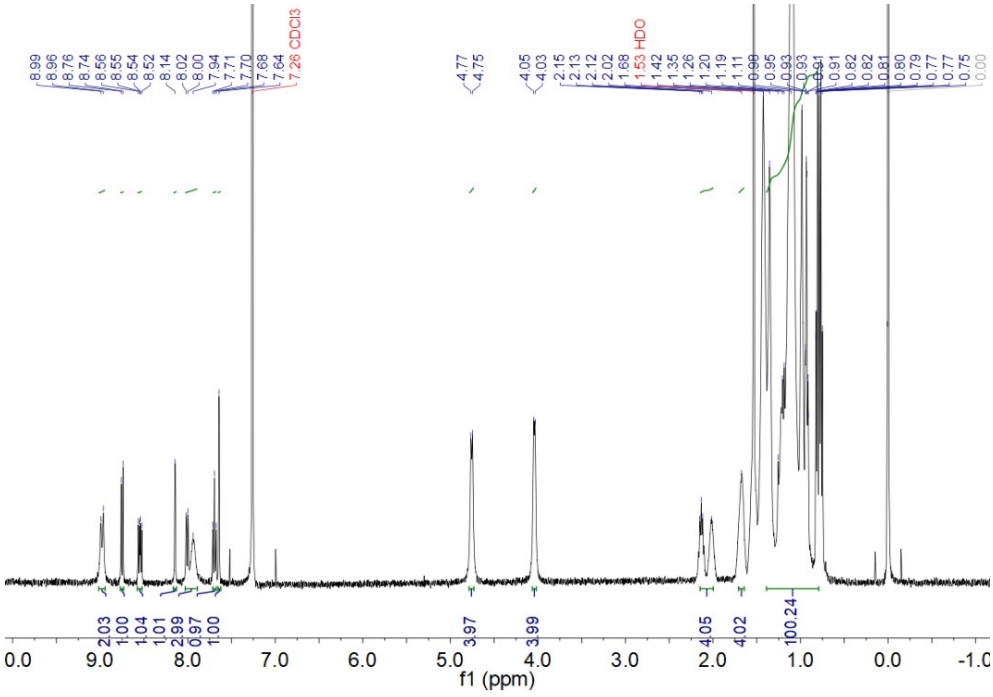

Figure S7. ^{1}H NMR spectrum of **DM-TH** in $CDCl_3$.

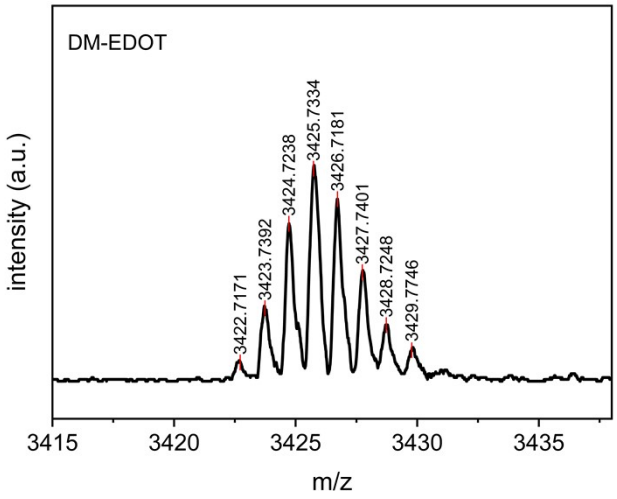

Figure S8. MALDI-TOF spectrum of **DM-EDOT**.

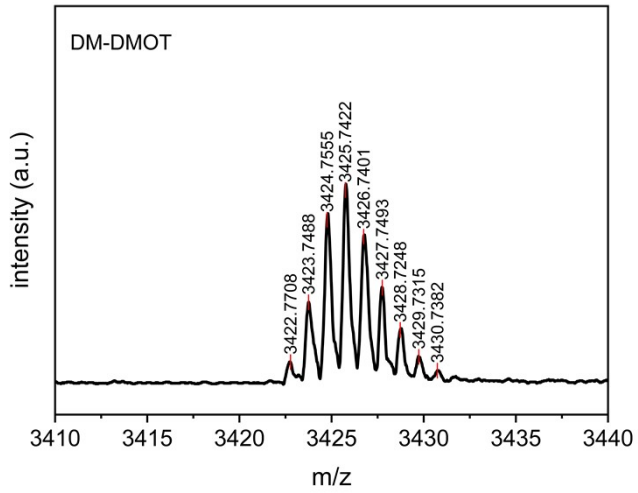

Figure S9. MALDI-TOF spectrum of **DM-DMOT**.

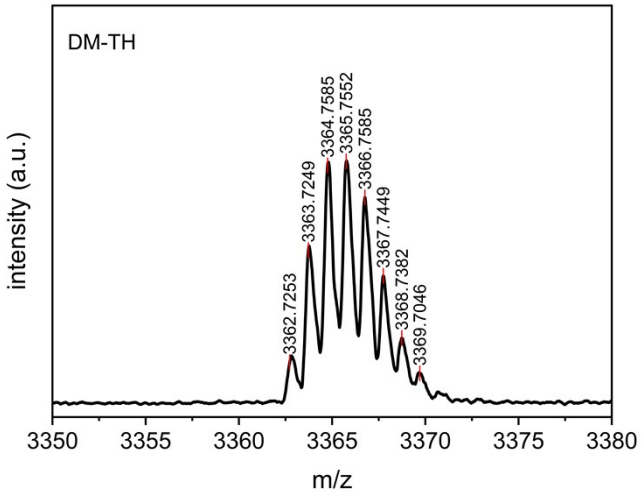

Figure S10. MALDI-TOF spectrum of **DM-TH**.

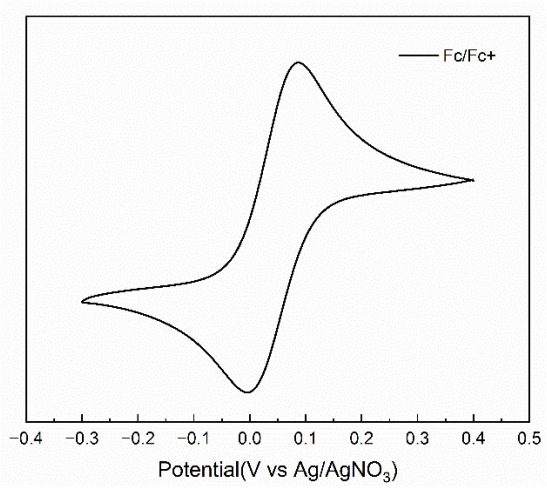

Figure S11. Cyclic voltammograms of Fc/Fc^{+}.

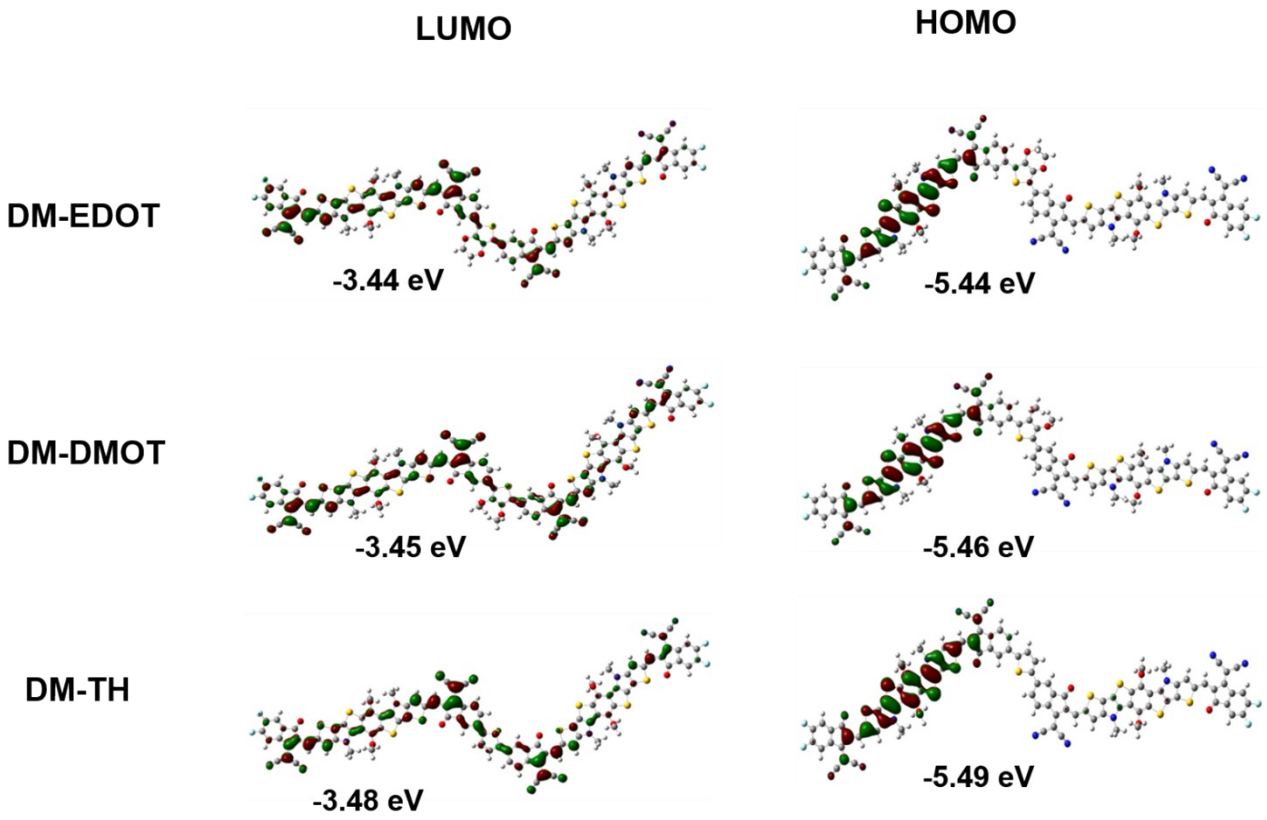

Figure S12. The energy levels of DM-EDOT, DM-DMOT, and DM-TH were calculated by the DFT method.

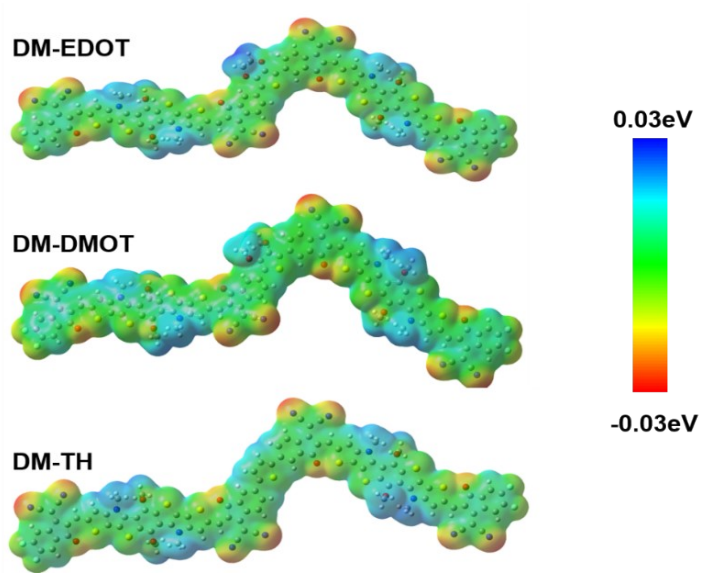

Figure S13. The electrostatic potential (ESP) of DM-EDOT, DM-DMOT, and DM-TH.

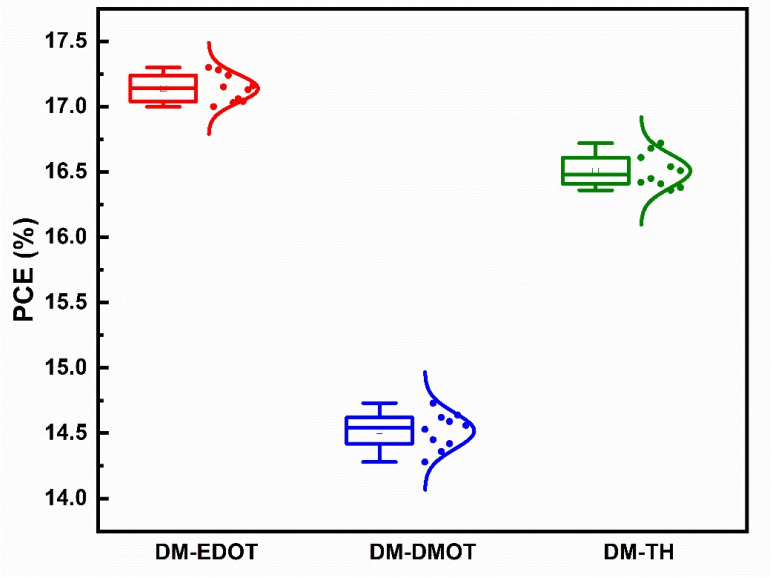

Figure S14. Statistical PCE distributions of DM-EDOT, DM-DMOT, and DM-TH measured from 10 individual devices.

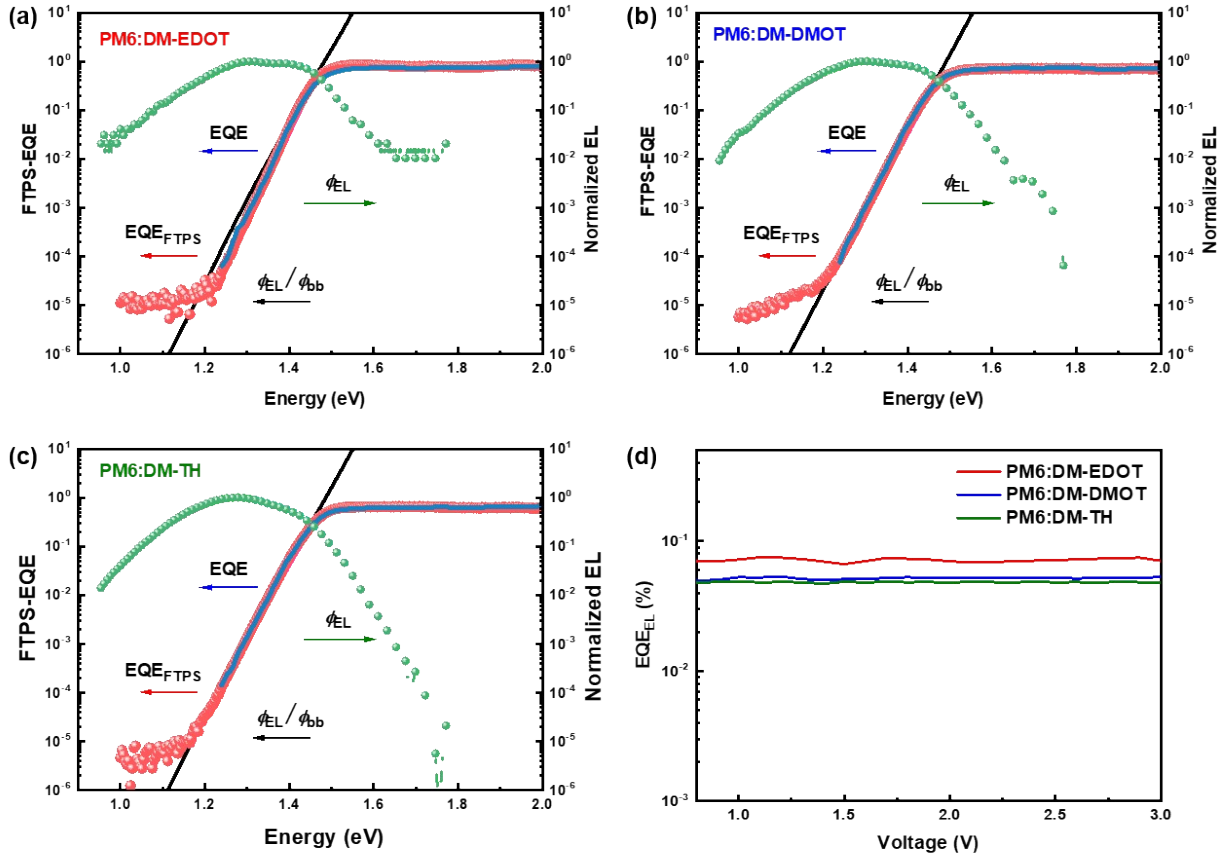

Figure S15. FTPS-EQE curves of the (a) PM6:DM-EDOT, (b) PM6:DM-DMOT, and (c) PM6:DM-TH blends. (d) EQE_{EL} for the OSCs.

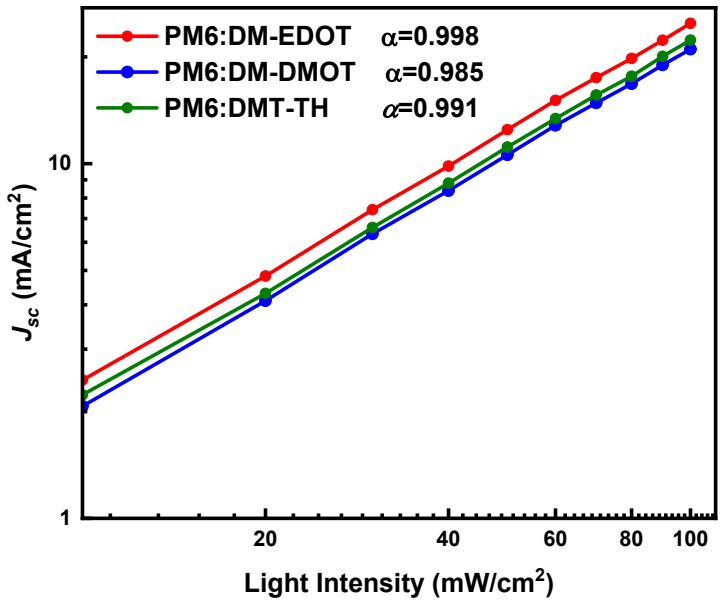

Figure S16. J_{sc} dependence on light intensity curves.

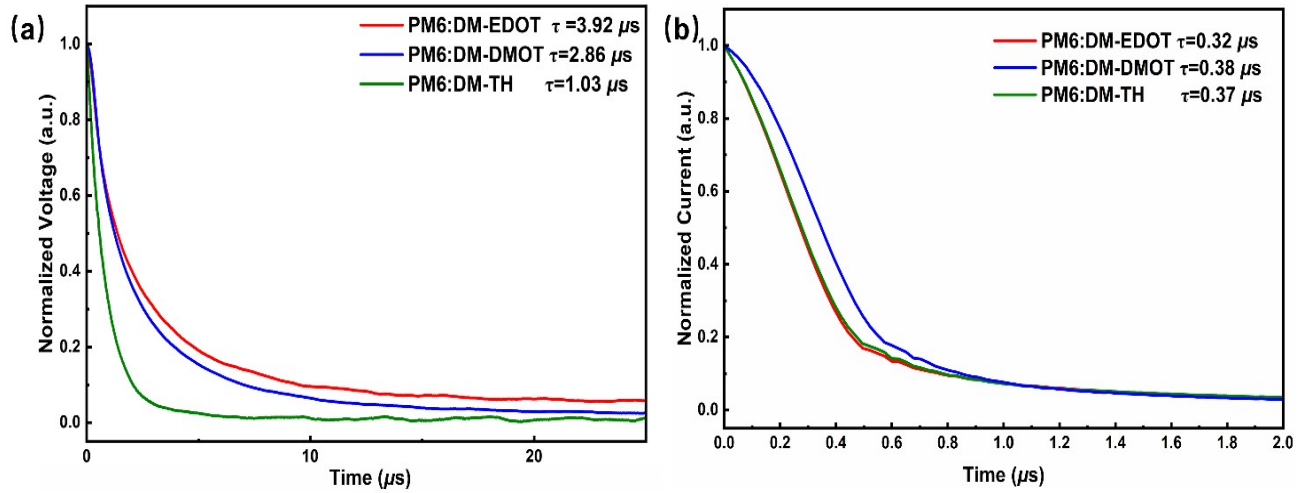

Figure S17. (a) Transient photovoltage (TPV) and (b) transient photocurrent (TPC) decay curves of the devices based on PM6:DM-EDOT, PM6:DM-DMOT, and PM6:DM-TH.

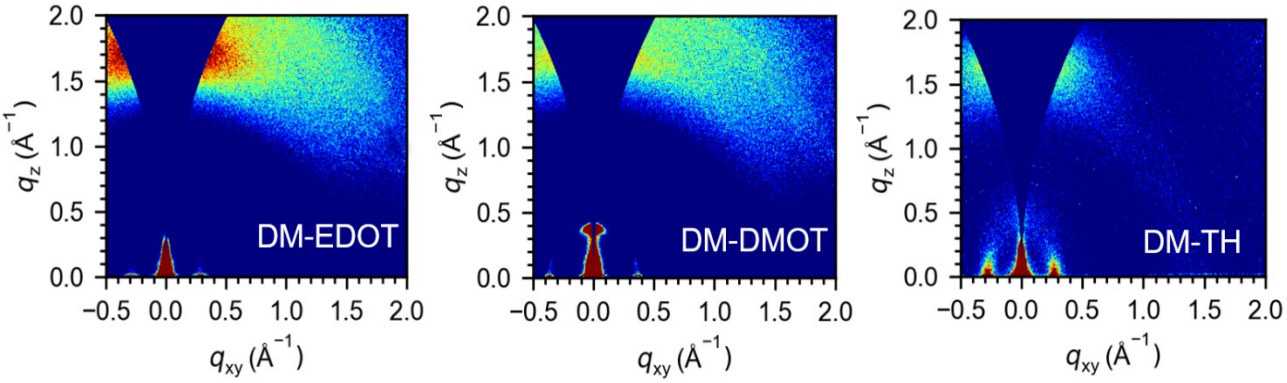

Figure S18. 2D-GIWAXS patterns of DM-EDOT, DM-DMOT and DM-TH neat films.

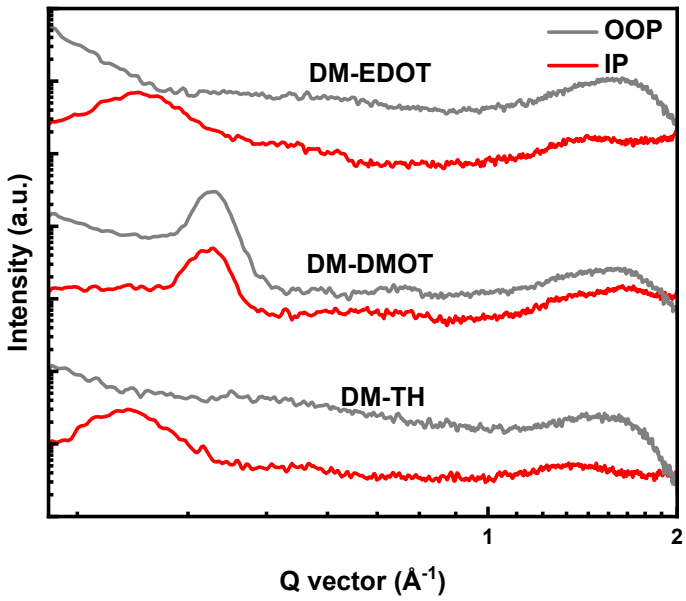

Figure S19. 1D extracted profiles of the corresponding 2D-GIWAXS patterns.

Table S1. PCEs and V_{oc} values of binary OSCs based on Y-series and ITIC-series DSMAs featuring electron-donating linkers in previous literatures.

Active layer	V_{oc} (V)	PCE (%)	Ref.
PM6:DM-EDOT	0.95	17.31	**This work**
PM6:GSNS-EH	0.949	17.34	*Adv. Mater.*, 2026, **38**, e18560
PM6:GSNS-C8	0.946	14.71	
PM6 : QM1	0.91	17.05	*Sci. China Chem.*, 2022, **65**, 1374-1382
PM6 : QM2	0.91	16.36	
PM6 : CH-D1	0.949	16.62	*Adv. Energy Mater.*, 2023, **13**, 2300301
PM6 : DIBP3F-S	0.901	16.11	*Angew. Chem. Int. Ed.*, 2023, **62**, e202302888
PM6 : DIBP3F-Se	0.917	18.09	
PM6 : DYT	0.94	17.30	*ACS Energy Lett.*, 2023, **8**, 1344-1353
PM6 : DYTVT	0.95	17.68	
PM6:DY-IDG	0.909	14.01	*Chem. Eng. J.*, 2025, **507**, 160416
PM6: G-DimerC8C10	0.907	15.20	*Small*, 2025, **21**, 2411698
D18:DYF-ThC4	0.975	12.88	*Adv. Funct. Mater.*, 2025, **35**, 2424978
D18:DY-FT	0.925	15.30	*ACS Energy Lett.*, 2024, **9**, 5541-5549
D18:DYF-E	0.938	17.02	*Adv. Funct. Mater.*, 2024, **34**, 2406501
D18:BC-Th	0.893	17.43	*Sci. China Chem.*, 2024, **67**, 1687-1696
PBQx-H-TF:dBSeNIC-γIC	0.880	17.68	*Adv. Funct. Mater.*, 2025, **35**, 2419453
P1:IDIC-T	0.95	8.34	*ACS Appl. Mater. Interfaces*, 2023, **15**, 27975-27983
P1:IDIC-TT	0.95	9.44	
PM6:DMT-HF	0.924	17.17	*Angew. Chem. Int. Ed.*, 2024, **50**, e202411155

Table S2. The detailed energy losses (E_{loss}) of the OSCs based on PM6:DM-EDOT, PM6:DM-DMOT, and PM6:DM-TH.

Devices	ΔE_1 [eV]	ΔE_2 [eV]	ΔE_3 [eV]	E_{loss} [eV]
PM6:DM-EDOT	0.234	0.073	0.183	0.490
PM6:DM-DMOT	0.268	0.069	0.192	0.529
PM6:DM-TH	0.270	0.067	0.194	0.531

Table S3. Summary of photovoltaic parameters for conventional and inverted devices based on three DSMAs prepared by different methods.

Active layer	Method	V_{oc} [V]	FF [%]	J_{sc} [mA cm^{-2}]	PCE [%]
PM6:DM-EDOT	Conventional BHJ	0.95	71.96	25.02	17.11
	Conventional LBL	0.95	72.87	24.99	17.31
	Inverted BHJ	0.95	70.98	21.57	14.54
	Inverted LBL	0.93	67.37	19.89	12.34
PM6:DM-DMOT	Conventional BHJ	0.94	69.73	21.58	14.21
	Conventional LBL	0.94	69.86	22.21	14.60
	Inverted BHJ	0.93	68.60	19.15	12.23
	Inverted LBL	0.92	65.41	17.83	10.65
PM6:DM-TH	Conventional BHJ	0.92	71.89	24.88	16.50
	Conventional LBL	0.93	72.98	24.52	16.72
	Inverted BHJ	0.92	70.73	20.11	13.13
	Inverted LBL	0.91	68.37	18.51	11.50

Table S4. The parameters of diffraction peaks from GIWAXS line-cuts in out-of-plane and in-plane directions.

Films	In-plane (100)				Out of plane (010)			
	q_z[Å^{-1}]	*d*-spacing [Å][a]	FWHM [Å^{-1}]	CCL [Å][b]	q_z[Å^{-1}]	*d*-spacing [Å][a]	FWHM [Å^{-1}]	CCL [Å][b]
DM-EDOT	0.277	22.67	0.039	144.92	1.631	3.85	0.376	15.02
DM-DMOT	0.365	17.21	0.040	141.30	1.564	4.02	0.384	14.69
DM-TH	0.267	23.52	0.038	147.57	1.433	4.39	0.310	18.23
PM6:DM-EDOT	0.269	23.35	0.056	100.93	1.728	3.63	0.259	21.77
PM6:DM-DMOT	0.276	22.75	0.064	88.31	1.713	3.66	0.285	19.83
PM6:DM-TH	0.280	22.43	0.068	83.12	1.709	3.67	0.262	21.57

[a] Calculated from the equation: $d = 2\pi/q$. [b] Obtained from the Scherrer equation: $CCL=2\pi K/\text{FWHM}$, where FWHM is the full-width at half-maximum and K is a shape factor (K= 0.9 here).

Table S5. The film thicknesses (d), hole (μ_h) mobilities, and electron (μ_e) mobilities of PM6:DM-EDOT, PM6:DM-DMOT, and PM6:DM-TH blend films.

Films	d [nm][a]	μ_h [$\times 10^{-4}$ cm^2 V^{-1} s^{-1}]	d [nm][b]	μ_e [$\times 10^{-4}$ cm^2 V^{-1} s^{-1}]	μ_e/μ_h
PM6:DM-EDOT	103	8.43	110	8.71	1.03
PM6:DM-DMOT	100	4.38	100	5.23	1.19
PM6:DM-TH	99	4.17	96	6.47	1.55

[a] Film thicknesses of the hole-only devices. [b] Film thicknesses of the electron-only devices

References

[S1] Y. Zhu, Y. Ma, L. Liu, D. Cai, J. Y. Wang, H. Shi and Q. Zheng, *Angew. Chem. Int. Ed.*, 2024, 63, e202411155.

[S2] Y. Ma, M. Zhang, S. Wan, P. Yin, P. Wang, D. Cai, F. Liu and Q. Zheng, *Joule*, 2021, 5, 197-209.